sensors

MDPI

Article

In Situ Pipe Prover Volume Measurement Method

Jiacheng Hu *, Weikang Zhou, Aijun Chen, Jiale Cai, Jing Yu, Zhengzhiyong Cui and Dongsheng Li

College of Metrology and Measurement Engineering, China Jiliang University, Hangzhou 310018, China; 18897827504@163.com (W.Z.); chenaijun@cjlu.edu.cn (A.C.); a534987977@163.com (J.C.); yujing@cjlu.edu.cn (J.Y.); cuizhengzy0204@163.com (Z.C.); lidongsheng@cjlu.edu.cn (D.L.)
* Correspondence: hujiacheng@cjlu.edu.cn

Abstract: To improve the accuracy of in situ measurement of the standard volumes of pipe provers and to shorten the traceability chain, a new method of in situ pipe prover volume measurement was developed alongside a supporting measurement device. This method is based on the geometric dimension approach, which measures the inner diameter and length of a pipe prover to calculate its volume. For inner diameter measurement, a three-probe inner-diameter algorithm model was established. This model was calibrated using a standard ring gauge of Φ313 mm, with the parameters calculated through fitting. Another standard ring gauge of Φ320 mm was used to verify the inner diameters determined by the algorithmic model. A laser interferometer was employed for the segmented measurement of the pipe prover length. The comprehensive measurement system was then used for in situ measurement of the standard pipe prover. The newly developed system achieved an expanded uncertainty of 0.012% (k = 2) in volume measurement, with the deviation between the measured and nominal pipe prover volumes being merely 0.007%. These results demonstrate that the proposed in situ measurement method offers ultra-high-precision measurement capabilities.

Keywords: dimensional method; geometry measurement; volume of pipe prover; measurement uncertainty

Citation: Hu, J.; Zhou, W.; Chen, A.; Cai, J.; Yu, J.; Cui, Z.; Li, D. In Situ Pipe Prover Volume Measurement Method. *Sensors* **2024**, *24*, 4873. https://doi.org/10.3390/s24154873

Academic Editor: Han Haitjema

Received: 20 June 2024
Revised: 20 July 2024
Accepted: 24 July 2024
Published: 26 July 2024

1. Introduction

As essential trade-measuring instruments [1], standard pipe provers are widely used in the oil and gas industry for trade transactions. Volume deviations in pipe provers can lead to unfair trade practices and significant economic losses. Moreover, pipe provers serve as industrial calibration devices [2], crucial for the production, transportation, and storage of oil and gas. Any deviation in their volume calibration can hinder the detection of issues during these processes, such as oil leakage and seepage, potentially causing serious safety accidents and endangering lives and property. Therefore, ensuring the accurate calibration of pipe provers is of great significance.

Pipe prover measurement methods primarily include the volumetric method, gravimetric method, and master meter proving solution. The volumetric method uses a certified volumetric tank prover [3] as a standard measuring tool and calculates the volume of the pipe prover based on the measured liquid level, density, and temperature of the volumetric tank [4]. This method necessitates tracing the volumetric tank as an intermediate transfer standard, accomplished through the dimensional method [5]. In addition, the shape and appearance of the volumetric tank can affect the measurement [6], which imposes significant limitations on the volumetric method.

The gravimetric method involves filling the pipe prover with an intermediate medium, discharging the medium into a gravimetric tank, and then weighing the medium. This method uses the weight of the medium to convert the volume of the pipe prover, utilising standard scales and weights as standard measuring tools.

In 2016, Doihara used a gravimetric tank and piston to measure the volume of a pipe prover, achieving an expanded uncertainty of 0.066% (k = 2) [7]. However, this method

imposes strict requirements on the calibration process. During measurement, pressure and temperature can vary rapidly and unevenly, while the viscosity and density of the medium significantly affect measurement accuracy [8]. Consequently, correcting the measurement results is crucial [9]. The master meter proving solution employs a standard flow meter as the transfer standard between the pipe prover and the measuring instrument, using flow parameters to indirectly measure the pipe prover volume. In 2015, Shimada verified the volume of a pipe over 15 m long with an inner diameter of 150 mm using the master meter method. The expanded uncertainty of the volume flow rate reached 0.03%, and the uncertainty of the mass flow rate reached 0.02% (k = 2) [10]. In the same year, the National Metrology Institute of the Netherlands used a standard flow meter to calibrate a 500 L volume tank, achieving an expanded volume measurement uncertainty of less than 0.04% (k = 2). However, verifying the stability and continuity of a standard flow meter through actual measurements is challenging, making cumulative errors difficult to avoid [11].

After analysing the uncertainty of the volume tube used in the volumetric method, Lim [12] and Oracheski [13] believed that the standard volume tank itself played a dominant role. This greatly limits the further improvement of the volumetric measurement accuracy. When the mass method measures small volumes, it is limited by the principle of mass measurement, and the measurement accuracy is difficult to improve further. When Toshihiro Morioka and others used the standard flow meter method for measurement, the relative measurement uncertainty of the standard flow meter itself reached 0.09%, and in the case of large fluctuations [14], the relative measurement uncertainty reached 0.44%. In addition, the standard flow meter can usually obtain good measurement accuracy in the low flow area, but it is difficult to obtain high accuracy in the high flow area [15]. These methods indirectly measure the pipe prover volume through intermediate media, which inevitably extends the traceability chain to the SI unit [16]. The length of the traceability chain directly impacts measurement accuracy, significantly limiting the efficacy of these methods. Therefore, reducing the traceability chain length in pipe prover volume measurement is crucial for improving accuracy.

The dimensional method is an in situ approach that calculates the pipe prover volume by measuring the length and inner diameter of a standard pipe prover segment. This method can be directly traced to the length benchmark, significantly improving measurement accuracy. In 2003, Többen developed an axial and radial incremental length measurement device and used it to measure the geometric quantity of a pipe prover with a nominal volume of 250 L. The measured volume was compared with that obtained using the gravimetric method, with a difference of only 0.008% [17]. Többen was the first to use the dimensional method to measure a pipe prover, demonstrating the potential of this method for a more accurate characterisation of pipe prover volumes. Compared with traditional measurement methods, this method is less susceptible to external factors and has looser environmental requirements. With the continuous improvement of geometric measurement accuracy, the dimensional method has more advantages in measuring the volume of a pipe prover.

The feasibility of using the dimensional method to measure pipe provers has been verified in previous studies. However, when using dual probes to measure the inner diameter, possible installation deviations of the sensor, such as the installation angle and eccentric distance, have been ignored. The influence of factors such as the eccentric distance and the lack of measurement uncertainty analysis in this method make verifying the reliability of this measurement method challenging. Therefore, this paper proposes a new method for pipe prover volume detection. In this approach, three probes are used to measure the inner diameter. An inner diameter algorithm model is utilised that includes installation angle, eccentric distance, and measured arm length parameters. The length is measured using a laser interferometer. A supporting measurement device is employed to complete the in situ measurement and uncertainty analysis of the pipe prover volume.

2. Measurement Method

A pipe prover is a hollow cylinder measuring instrument with a segmented design. In this study, the pipe prover was divided into multiple standard segments using a detection switch. Consequently, the pipe prover volume measurement is based on the addition of the volumes of multiple segments, as shown in Equation (1):

$$\begin{cases} V_i = \pi \times \left(\frac{\mathrm{DP}_i}{2}\right)^2 \times \mathrm{LP}_i \\ V = \sum_{i=1}^{4} V_i \end{cases} (i = 1, 2, 3, 4), \quad (1)$$

where, DP_i, LP_i, and V_i represent the inner diameter, length, and volume of each standard segment of the pipe prover, respectively, and V is the total volume of the standard segments of the pipe prover. The calculation principle for the pipe prover volume is illustrated in Figure 1. The inner diameter and length of the pipe prover must be measured separately. High-precision measurements of the inner diameter of a pipeline are typically performed by measuring the relative displacement of the sensor [18]. This method cannot directly obtain the inner diameter of the measured object; therefore, an inner diameter algorithm model must be established, followed by using the relative measurement value of the sensor to calculate the inner diameter of the pipe. Segmented length measurements were required in this study because the pipe prover had a segmented design.

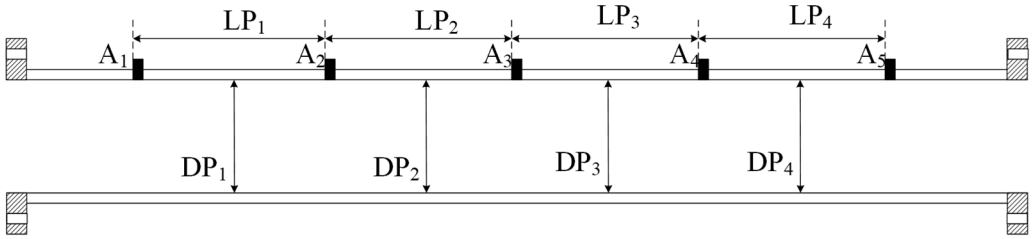

Figure 1. Pipe prover volume calculation method.

2.1. Inner Diameter Measurement Method

The inner diameter measurement method was based on the three-point circle principle [19], as shown in Figure 2. Under ideal conditions, three coplanar laser displacement sensors installed at angles of 120° with respect to one another are used to measure the distance from the wall of the pipe prover. The distances between the measurement points of sensors form a triangle, and the radius of its circumscribed circle is determined.

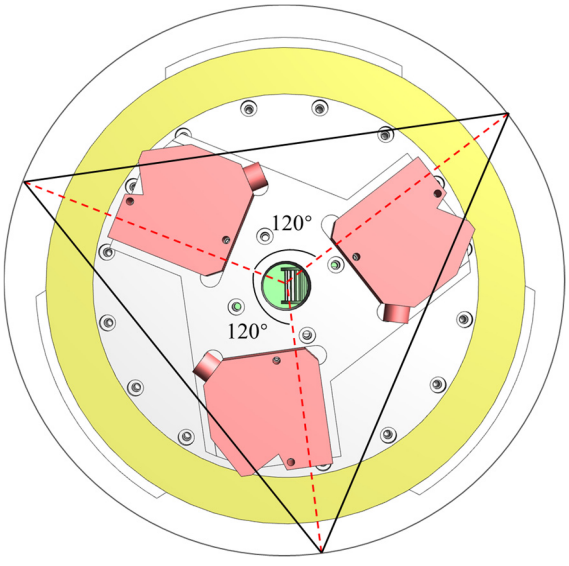

Figure 2. Principle of three-point circle determination.

However, in an actual measurement environment, deviations in the installation angles of the three laser displacement sensors will exist, meaning the angles between the sensors are not precisely 120°. Considering that the actual rotation centre of the three sensors will differ from that of the measured pipe prover, the centres of the circles do not coincide, causing a deviation between the axis of each sensor and the centre of the circle. The three-probe inner-diameter algorithm model based on this scenario is shown in Figure 3.

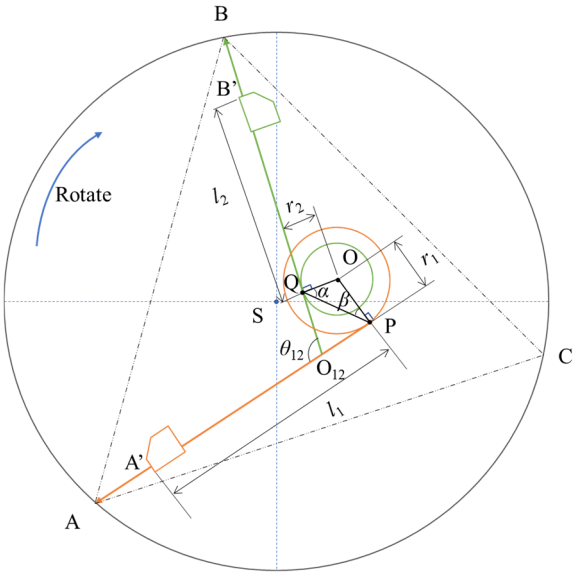

Figure 3. Principle of three-probe inner diameter algorithm model.

In Figure 3, A' and B' are the measurement starting points of the laser displacement sensors, S is the centre of the circle of the measured pipe prover, O is the actual rotation centre of the inner diameter measurement module, O_{12} is the intersection point of measurement beams AA' and BB', and θ_{12} is the angle between the measurement beams. During rotation measurement, taking measurement beams AA' and BB' as examples, each beam rotates around point O, forming two concentric tangent circles of the beam. OQ and OP are the radii of the tangent circles, denoted as r_1 and r_2, respectively. $A'P$ and $B'Q$ are the distances from the measurement starting point to the installation starting point, denoted as l_1 and l_2, respectively. α and β are the angles for auxiliary calculation, expressed as $\alpha = \angle OQP$ and $\beta = \angle OPQ$, respectively.

In the three-probe inner diameter algorithm model, the unique triangle ABC formed by the measurement points can be obtained. The side length AB in the triangle can be calculated using the cosine theorem:

$$AB = \sqrt{O_{12}A^2 + O_{12}B^2 - 2 \cdot O_{12}A \cdot O_{12}B \cdot \cos\theta_{12}}. \tag{2}$$

$O_{12}A$ and $O_{12}B$ can be expressed as

$$\begin{cases} O_{12}A = l_1 + AA\prime - O_{12}P \\ O_{12}B = l_2 + BB\prime + O_{12}Q \end{cases}, \tag{3}$$

where AA' and BB' are the measured values of the sensor and l_1 and l_2 are the lengths of the measuring arms. Therefore, AB can be calculated by determining $O_{12}P$ and $O_{12}Q$.

In triangle OPQ, it can be known from the sine formula:

$$\frac{\sin\alpha}{r_2} = \frac{\sin\beta}{r_1} = \frac{\sin\theta_{12}}{PQ}. \tag{4}$$

α and β in Equation (4) can be obtained as

$$\begin{cases} \beta = \sin^{-1}\left(r_1 \frac{\sin\theta_{12}}{PQ}\right) \\ \alpha = \sin^{-1}\left(r_2 \frac{\sin\theta_{12}}{PQ}\right) \end{cases}. \tag{5}$$

In the quadrilateral $OQO_{12}P$, PQ is also obtained from the cosine formula:

$$PQ = \sqrt{{r_1}^2 + {r_2}^2 - 2 \cdot r_1 \cdot r_2 \cdot \cos\theta_{12}}, \tag{6}$$

and in triangle $O_{12}PQ$, it can be found by using the sine formula:

$$\frac{\sin(\frac{\pi}{2} - \alpha)}{O_{12}P} = \frac{\sin(\frac{\pi}{2} - \beta)}{O_{12}Q} = \frac{\sin(\pi - \theta_{12})}{PQ}. \tag{7}$$

$O_{12}P$ and $O_{12}Q$ in Equation (7) can be obtained by applying

$$\begin{cases} O_{12}Q = PQ\frac{sin\left(\frac{\pi}{2} - \alpha\right)}{sin(\pi - \theta_{12})}, \\ O_{12}P = PQ\frac{sin\left(\frac{\pi}{2} - \beta\right)}{sin(\pi - \theta_{12})}. \end{cases} \tag{8}$$

By substituting Equations (5) and (6) into Equation (7), $O_{12}P$ and $O_{12}Q$ can be calculated. Side length AB can be calculated using Equations (2) and (3), and similarly for side lengths BC and CA.

R can be obtained from the formula for the radius of the circumscribed circle of a triangle as follows:

$$\begin{cases} P = \frac{AB+BC+CA}{2} \\ AB = \sqrt{O_{12}A^2 + O_{12}B^2 - 2 \cdot O_{12}A \cdot O_{12}B \cdot \cos\theta_{12}} \\ BC = \sqrt{O_{23}B^2 + O_{23}C^2 - 2 \cdot O_{23}B \cdot O_{23}C \cdot \cos\theta_{23}} \\ CA = \sqrt{O_{31}C^2 + O_{31}A^2 - 2 \cdot O_{31}C \cdot O_{31}A \cdot \cos\theta_{31}} \\ R = \frac{AB \cdot BC \cdot CA}{4\sqrt{P(P-AB)(P-BC)(P-CA)}} \\ D = 2R \end{cases} \tag{9}$$

AB, BC, and CA are calculated by AA', BB', CC', θ_{12}, θ_{23}, θ_{31}, l_1, l_2, l_3, r_1, r_2, and r_3. The inner diameter D of the smallest circumscribed circle of triangle ABC can be expressed as

$$D = f\left(l_1, l_2, l_3, r_1, r_2, r_3, \theta_{12}, \theta_{23}, \theta_{31}, AA', BB', CC'\right) \tag{10}$$

The measured pipe volume was divided into four segments in this study. When measuring the first segment, the inner diameter calculated using the three-probe inner diameter algorithm model represented the inner diameter of a single sampling point in a single section. To accurately reflect the inner diameter of a single section n sampling measurements were conducted to obtain D_{11j} (j = 1, 2, 3, …, n). However, the inner diameter of a single section cannot accurately represent the inner diameter of a pipe segment. Therefore, m cross-sectional measurements were performed on this pipe segment, resulting in D_{1ij} (i = 1, 2, 3, …, m; j = 1, 2, 3, …, n). The average of these sampled measurements, D_1, was used as the inner diameter of the first segment of the pipe prover:

$$D_1 = \sum_{i,j=1}^{m,n} \frac{1}{n \times m} D_{1,i,j} (i = 1, 2, 3, \cdots, m; j = 1, 2, 3, \cdots n) \tag{11}$$

The inner diameters D_2, D_3, and D_4 of the remaining three pipe segments were calculated using the same method.

2.2. Length Measurement Method

The length of the pipe prover was measured using a laser interferometer. Detection switches were present at both ends of each segment of the pipe prover. A trigger was installed on the measurement device to activate the detection switch. When the first segment was measured, detection was triggered, and the reading of the laser interferometer was recorded. The difference in the readings of the laser interferometer at both ends of the segment, activated by the detection switch, was taken as the length L_1 of the first segment of the pipe prover:

$$L_1 = |L_{11} - L_{12}|. \tag{12}$$

L_2, L_3, and L_4 of the remaining three pipe segments of the volume pipe were calculated using the same method.

3. Experimental Setup

The experimental device, shown in Figure 4 consists of an inner diameter measurement module (Figure 5), a length measurement module (Figure 6), and a motion control module (Figure 7).

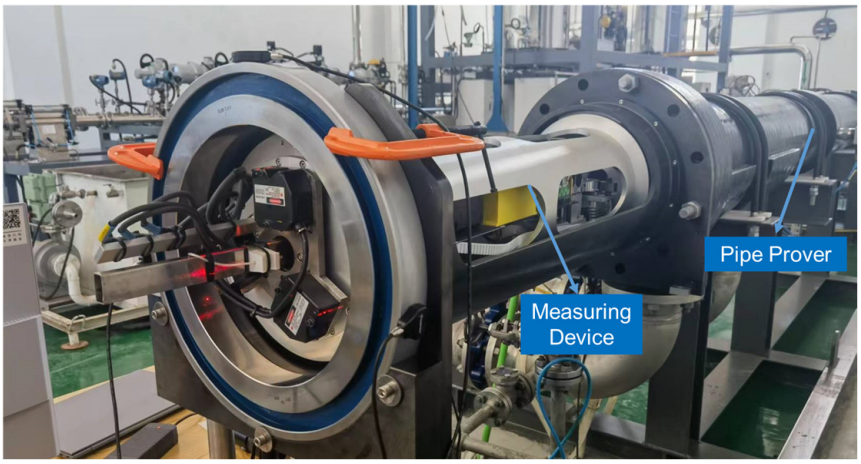

Figure 4. Experimental setup.

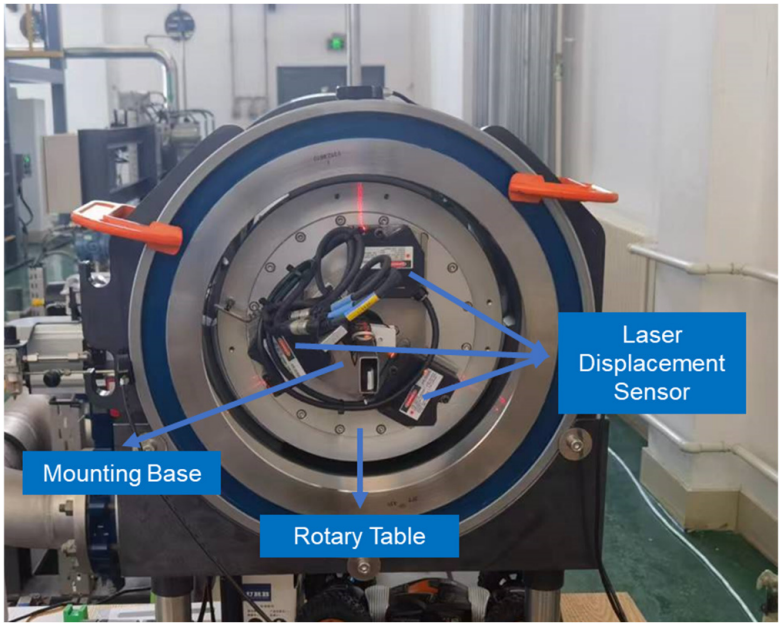

Figure 5. Diameter measurement module.

Figure 6. Length measurement module.

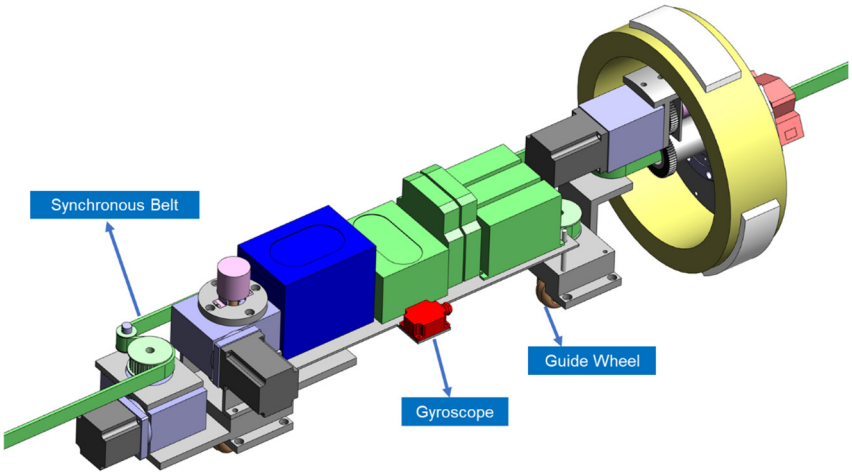

Figure 7. Motion and posture adjustment module.

3.1. Inner Diameter Measurement Module

The inner diameter measurement module, developed based on the three-point circle principle, is shown in Figure 5. This module mainly comprises a rotating stage and three laser displacement sensors. The three laser displacement sensors are installed at angles of 120° relative to one another. Each sensor is positioned equidistantly from the centre of rotation and fixed on the mounting base, which rotates with the rotary table. The entire inner diameter measurement module moves within the pipe prover along with the measurement device, enabling the measurement of different sections of the pipe prover.

The laser displacement sensor used to measure the inner diameter is a KEYENCE sensor, with a measurement accuracy of 2 μm and a measurement range of ±10 mm, which meets the requirements for inner diameter measurement accuracy and range. To improve the accuracy of the inner diameter measurement, an electric rotary table from IKO is utilised, with both axial and radial runout less than 5 μm.

3.2. Length Measurement Module

The length measurement module is shown in Figure 6. This module primarily consists of a laser interferometer fixed at one end of the pipe prover, while the reflector is attached

to the measurement device. The measurement device triggers the detection switch between each pipe segment, synchronously recording data from the laser interferometer and completing the length measurement of each pipe segment through the device's movement.

The laser interferometer is a CHOTEST single-frequency interferometer with a length measurement accuracy of up to 0.5 ppm, accommodating a length measurement range of up to 40 m. To ensure stable movement of the laser interferometer mirror and maintain a continuous and uninterrupted light path, we specially designed PTFE [20] blocks surrounding both sides of the measurement device. Springs are installed inside the PTFE blocks to expand outward, achieving a fit between the measurement device and the inner wall of the pipe. This setup ensures precise and accurate in situ measurements of both the inner diameter and length of the pipe prover segments, significantly enhancing the reliability of the overall volume measurement.

3.3. Motion Control Module

The motion control module, shown in Figure 7, primarily comprises a synchronous belt, gyroscope, and guide wheel. The synchronous belts are fixed at both ends of the pipe prover, allowing the measurement device to move along the belt.

The gyroscope is a WitMotion attitude sensor, with an inclination accuracy of 0.001° and a measurement range of ±90°, meeting the operational requirements. To avoid the effects of pitch and yaw angles on the inner diameter and length measurement results during movement, the gyroscope continuously reads the attitude information of the measurement device. This allows the motion control module to control the device in real time.

4. Experiments and Results

4.1. Experimental Pipe Prover

A standard pipe prover was selected as the measurement object, divided into four standard segments: P_1, P_2, P_3, and P_4. The nominal volumes of these segments, based on the design indicators of the pipe prover, are listed in Table 1.

Table 1. Nominal volumes of pipe prover segments.

Pipe Segments	Volume (dm^3)
P_1	150.76
P_2	150.80
P_3	150.67
P_4	150.55
P_1–P_4	602.78

The pipe prover to be measured is made of glass-fibre-reinforced epoxy resin material, with a total length of approximately 12 m. Two buffer segments, approximately 1 m long each, are present at both ends of the pipe prover, with a standard pipe segment approximately 8 m long in the middle. As shown in Figure 8, detection switches A_1, A_2, A_3, A_4, and A_5 are located at the beginning and end of pipe segments P_1, P_2, P_3, and P_4.

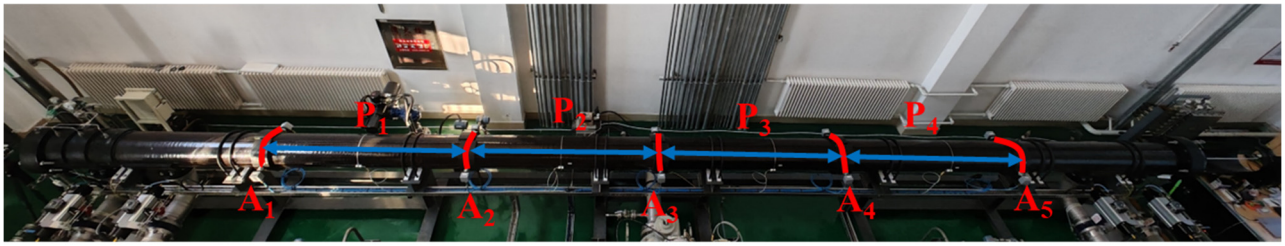

Figure 8. Standard pipe prover.

The experimental site has the ability to regulate temperature. During the entire experiment, the temperature range of the volume tube and the measuring device is 20 ± 2 °C.

4.2. Calibration of Inner Diameter Three-Probe Algorithm Model

According to the three-probe inner diameter algorithm model described by Equation (10), the inner diameter of the measured section was calculated using 12 parameters. However, in the actual measurement, only three of these parameters—AA′, BB′, and CC′ of the laser displacement sensor—are measured. These parameters can be obtained through sensor readings and vary with the measurement position, while the remaining nine parameters remain constant after the device is installed.

Due to the use of a non-contact measurement method involving the laser displacement sensor, measuring the angle between the optical path of the laser displacement sensor and the origin is challenging. Consequently, angles θ_{12}, θ_{23}, and θ_{31} as well as offsets r_1, r_2, and r_3 can only be determined by fitting the inverse solution. The lengths of the measuring arms along with a known minimum circumscribed circle inner diameter D of the triangle, must also be provided for Equation (10), so that θ_{12}, θ_{23}, and θ_{31} and r_1, r_2, and r_3 can be solved through fitting.

Since the number of unknown parameters affects the accuracy of the fitted inverse solution [21], an increase in unknown parameters reduces the degree of fitting. After comprehensive consideration, the included angle and offset distance [22] which have greater impacts on the measurement results, were selected as the unknown parameters.

Two standard ring gauges composed of bearing steel were machined as standard values for the inner diameter algorithm model. The nominal sizes of these gauges were Φ313 mm and Φ320 mm. The Φ313 mm standard ring gauge is shown in Figure 9.

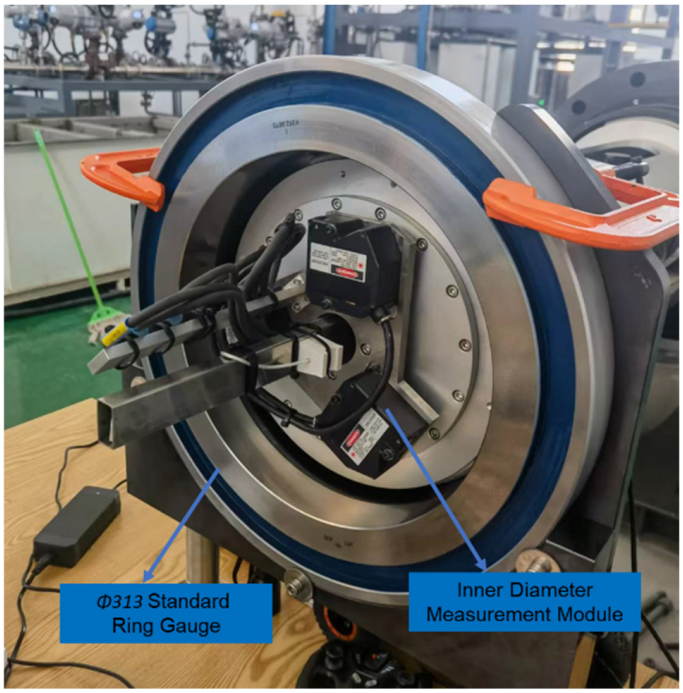

Figure 9. Φ313 mm standard ring gauge.

The parameters of the Φ313 mm standard ring gauge were obtained after metrological verification and are listed in Table 2.

Table 2. Φ313 mm ring gauge parameter.

Ring Gauge Position	Inside Diameter (mm)	Uncertainty k = 2 (mm)
Upper	312.9948	0.004
Middle	312.9950	0.004
Lower	312.9948	0.004

The ring gauge with a nominal size of Φ320 mm is shown in Figure 10.

Figure 10. Φ320 mm standard ring gauge.

The parameters of the Φ320 mm standard ring gauge were obtained after metrological verification and are listed in Table 3.

Table 3. Φ320 mm ring gauge parameters.

Ring Gauge Position	Inside Diameter (mm)	Uncertainty k = 2 (mm)
Upper	320.0002	0.004
Middle	320.0002	0.004
Lower	320.0002	0.004

The nominal value of the standard ring gauge is the standard length at a temperature of 20 °C. When using the standard ring gauge for calibration, temperature compensation must be performed on the inner diameter length of the standard ring gauge [23]. Considering that the material used in the standard ring gauge is bearing steel, the linear expansion coefficient α_R is 14 × 10^{-6}/°C, and the mounting base of the laser displacement sensor is made of Invar alloy, with a linear expansion coefficient α_{MD} of 0.8 × 10^{-6}/°C. When calibrating using the Φ313 mm standard ring gauge, the measurement device is in operation, causing the device to heat up slowly, which affects the temperature of both the standard ring gauge and the mounting base. During this period, the data were temperature-compensated to obtain the measured values of the three laser displacement sensors and the nominal values of the standard ring gauge. When the sampling angle interval between the sensors and the

standard ring gauge was 5°, each sensor measured 72 data points after one rotation. The obtained data are presented in Figure 11.

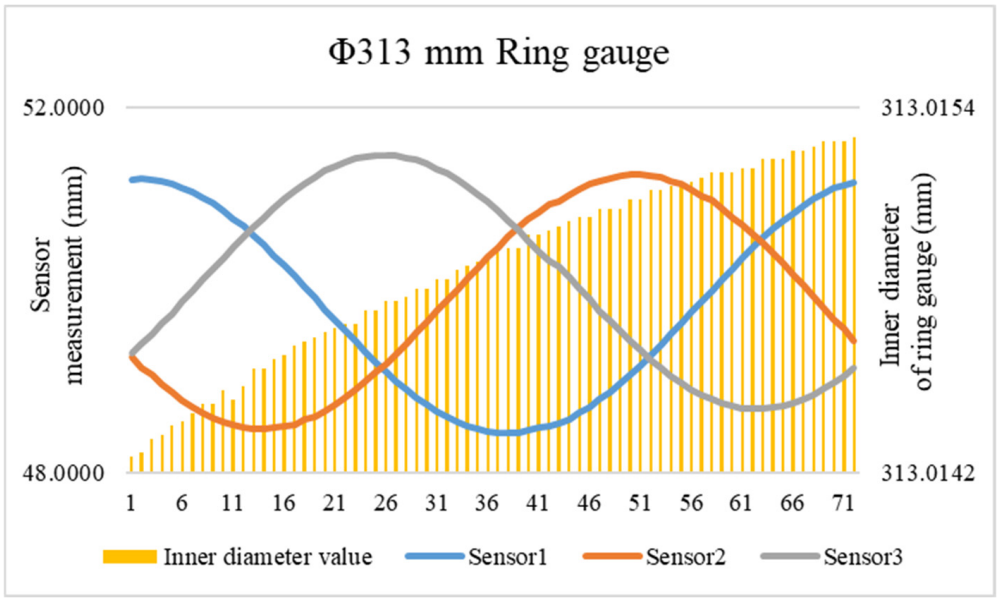

Figure 11. Data used for calibration.

Using this set of data for the fitting calculation of the inner diameter algorithm model, the values of each parameter of the inner diameter algorithm model were calculated and the fitting values were temperature-compensated. The parameter results are listed in Table 4.

Table 4. Fitting parameters.

Parameter	Value
l_1	106.4200 mm
l_2	106.8183 mm
l_3	106.4932 mm
θ_{12}	120.1452°
θ_{23}	119.7563°
θ_{31}	120.0985°
r_1	0.0857 mm
r_2	0.1152 mm
r_3	0.4601 mm

As the parameters of the inner diameter algorithm model are obtained through fitting and solving, certain errors must exist in the fitting values [24]. Therefore, the fitting effect of each parameter needs to be verified. For this purpose, a ring gauge (nominally Φ313 mm under the 20 °C standard condition) was used. The inner diameter of the standard ring gauge and that obtained from the inner diameter algorithm model were compared, as shown in Figure 12.

The quality of the fitting effect could not be verified using a single ring gauge. Additional data were required for verification [25]. For this purpose, a ring gauge (nominally Φ320 mm under the 20 °C standard condition) was used. The inner diameter of the standard ring gauge and that obtained from the inner diameter algorithm model were compared, as shown in Figure 13. The deviation between the average value of this data set and the standard value of the inner diameter is 1.50 μm, and the standard deviation is 1.37 μm.

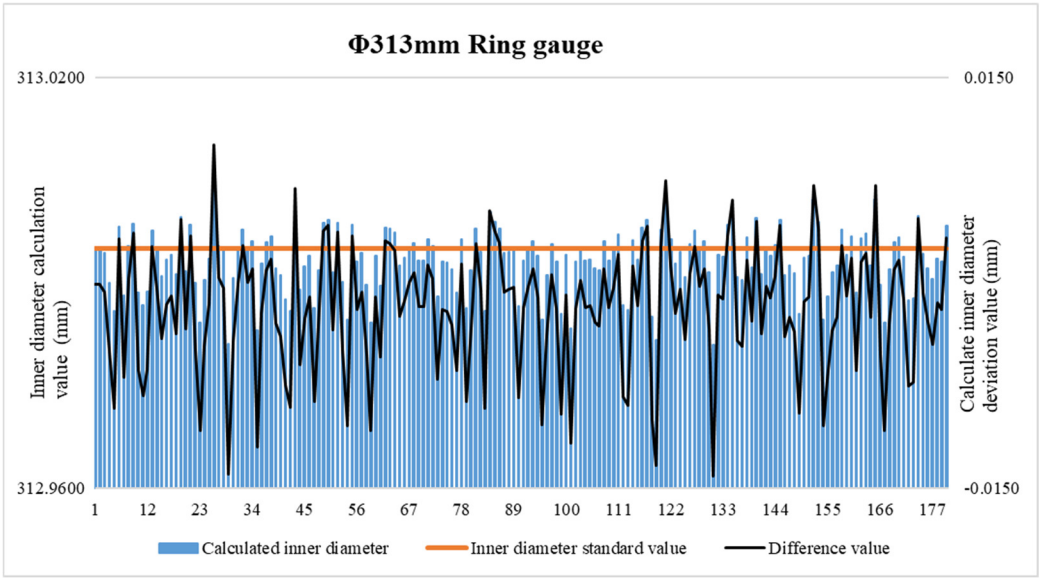

Figure 12. Φ313 mm ring gauge data used for verification.

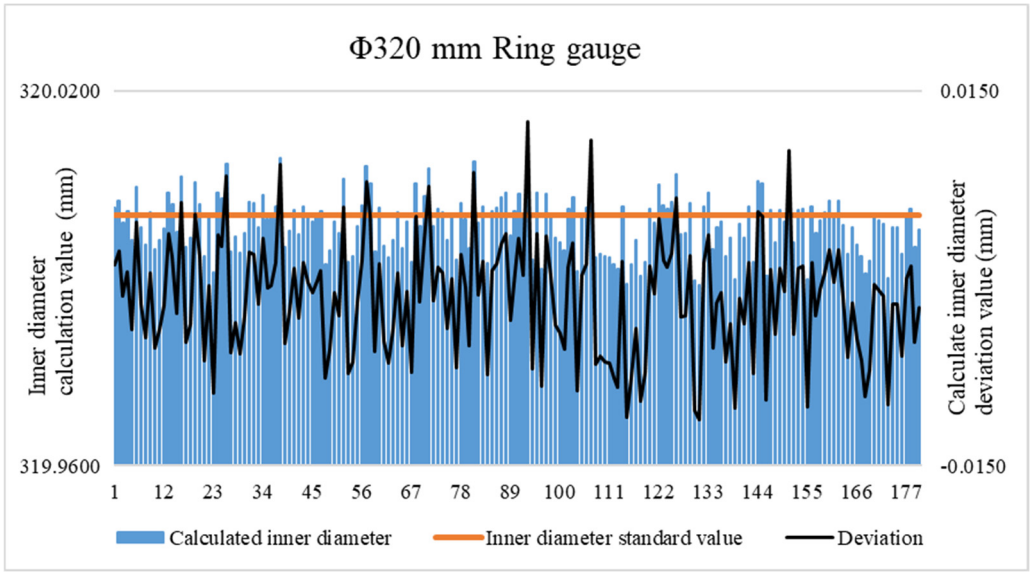

Figure 13. Data used for verification.

4.3. Inner Diameter Measurement Results

The pipe prover was measured in a 20 ± 2 °C environment, as shown in Figure 14.

During the measurements, the measurement device moved to standard pipe segment P_1 of the pipe prover and began measuring at the beginning of this segment. When measuring the first section, samples were taken at 20° intervals and repeated three times to complete the measurement of one section. The measurement device was then moved forward by 100 mm to measure the second section of the standard pipe segment, and the above steps were repeated until the inner diameter measurement of the standard pipe segment was completed. During the inner diameter measurement process, stabilization was performed for 5 s after each rotation of the sampling point to reduce the impacts of the axial and radial runouts of the turntable on the inner diameter measurement results.

The pipe prover is made of glass-fibre-reinforced epoxy resin, with a radial linear expansion coefficient α_{PD} of 34.6 × 10^{-6}/°C. The inner diameter of the pipe prover was temperature-compensated. The cross-sectional inner diameters obtained throughout the measurement process are presented in Table 5.

Figure 14. Inner wall of volume pipe.

Table 5. Pipe prover inner diameter measurements.

Pipe Segments	Temp (°C)	Inner Diameter of Pipe Segments (mm)
DP_1	25.38	314.3501
DP_2	24.28	314.2917
DP_3	25.11	314.2097
DP_4	24.12	314.1794

4.4. Length Measurement Results

The measurement device simultaneously measured the length of the inner diameter and the standard segment of the pipe prover in segments, and repeated the measurement on the detection switch of each segment 10 times. The axial linear expansion coefficient α_{PL} of the pipe prover is $17.3 \times 10^{-6}/°C$. The pipe prover length measurement results were temperature-compensated. The lengths of the pipe segments are listed in Table 6.

Table 6. Pipe prover length measurements.

Pipe Segments	Start Position (mm)	End Position (mm)	Revised Length (mm)
LP_1	2038.4513	3982.0110	1943.5597
LP_2	3990.5124	5931.1777	1940.6653
LP_3	5923.0308	7866.9834	1943.9526
LP_4	11,513.6269	13,456.1795	1942.5526

4.5. Volume Calculation Results

The volume of the pipe prover was calculated using the length and inner diameter of each segment, and the results are presented in Table 7.

Table 7. Pipe prover volume calculations.

Pipe Segments	Volume (dm^3)
P_1	150.84
P_2	150.58
P_3	150.74
P_4	150.60
P_1–P_4	602.74

According to Table 1, the standard volume V_{STD} of the pipe prover is 602.78 dm^3, whereas the volume V_{MEA} calculated after measuring the length and inner diameter of the pipe prover using the measurement device is 602.74 dm^3. Hence, the deviation V_{ERR} is 0.04 dm^3, the relative deviation V_{RSD} can be calculated to be 0.0066% by applying Equation (13):

$$V_{RSD} = \frac{V_{MEA} - V_{STD}}{V_{STD}} \times 100\% = \frac{V_{ERR}}{V_{STD}} \times 100\%. \quad (13)$$

5. Uncertainty Analysis

The uncertainty components for volumetric tube volume measurement can be described as follows.

(1) The uncertainty components of the inner diameter measurement include the (a) repeatability of the inner diameter measurement results, (b) indication error of the inner diameter measurement, (c) temperature compensation error of the standard ring gauge, (d) standard ring gauge linear expansion coefficient error, (e) standard ring gauge traceability, (f) inner diameter error of the measurement results caused by pipe roundness, (g) pipe prover radial temperature compensation error, (h) pipe prover radial linear expansion coefficient error, (i) pipe prover pressure deformation error, and (j) pipe prover hydraulic pressure deformation error.

(2) The uncertainty components of the length measurement include the (a) repeatability of the length measurement results, (b) laser interferometer measurement error, (c) signal delay error, (d) axial temperature change error, and (e) pipe prover axial linear expansion coefficient error.

5.1. Uncertainty Analysis of Inner Diameter Measurement

The inner diameter measurement results of multiple measurements of a single section of the volume tube are shown in Table 8. The standard deviation of the inner diameter measurement results is calculated to be 4.06 μm.

Table 8. Pipe prover single section inner diameter.

Number	Inner Diameter Value (mm)	Number	Inner Diameter Value (mm)
1	314.1697	6	314.1671
2	314.1735	7	314.1677
3	314.1616	8	314.1696
4	314.1701	9	314.1757
5	314.1731	10	314.1730

Because the inner diameter algorithm model utilises a three-point circle method, certain errors can occur when measuring the cross-section of a non-standard circle [26]. After assessing the full roundness of the standard segment of the pipe prover, the maximum roundness deviation was found to be 61.87 μm. To analyse the impact of this roundness deviation, a computer simulation was set up with a simulated circle having a roundness of 61.87 μm. Different measurement sampling intervals were tested, with simulations performed in 5° steps from 1° to 120°, covering a full 360° sampling of the simulated circle. The calculated inner diameter of each sampling point was obtained after inputting the

values into the algorithm model [27]. The average inner diameter of the simulated circle was then calculated, and the difference from the standard circle was noted. This process was repeated 100 times, each time setting a new roundness for the 61.87 µm simulation circle. The inner diameter deviations with respect to the sampling angle when measuring the simulation circle with a roundness of 61.87 µm are presented in Figure 15.

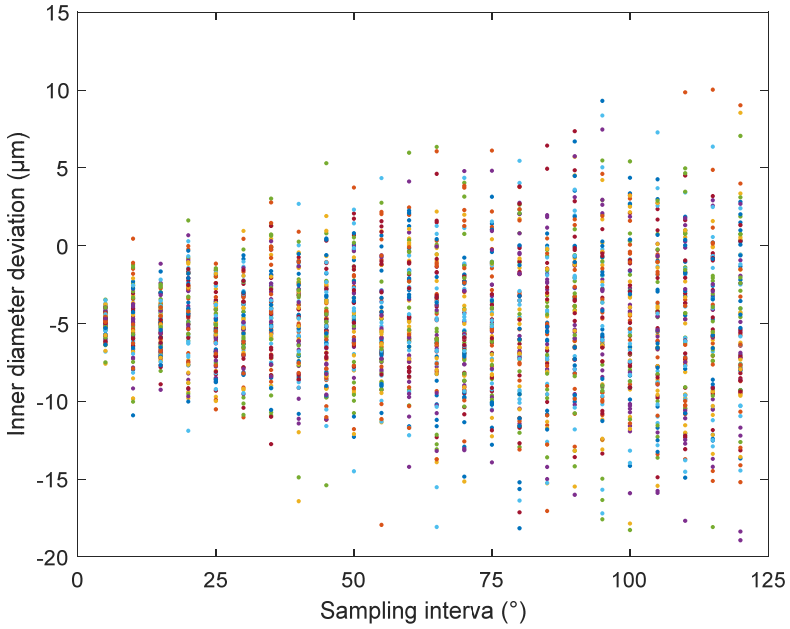

Figure 15. Influence of roundness on measurement.

The simulation results indicated that smaller sampling intervals led to a lower degree of inner diameter deviation but increased the measurement time. To balance measurement accuracy and efficiency, the sampling interval during the inner diameter measurement was set to 20°. Using a 95% confidence interval for the 20° sampling data set, the maximum deviation of this data set was 5.87 µm.

As the measurement device puts pressure on the tube wall when it is inside the pipe prover, the deformation of the tube wall under pressure must be considered. The simulation model was established and static analysis was performed based on the actual state of the measuring device when measuring the pipe prover. During the analysis, the parameters of the volume tube and blocks were set according to the mechanical properties of glass-fibre-reinforced epoxy resin material and PTFE, and the pressure was set according to the weight of the measuring device. The deformation of the pipe prover at the measurement section was evaluated, as shown in Figure 16. The error of the inner diameter measurement module caused by compression deformation was found to be 0.8 µm.

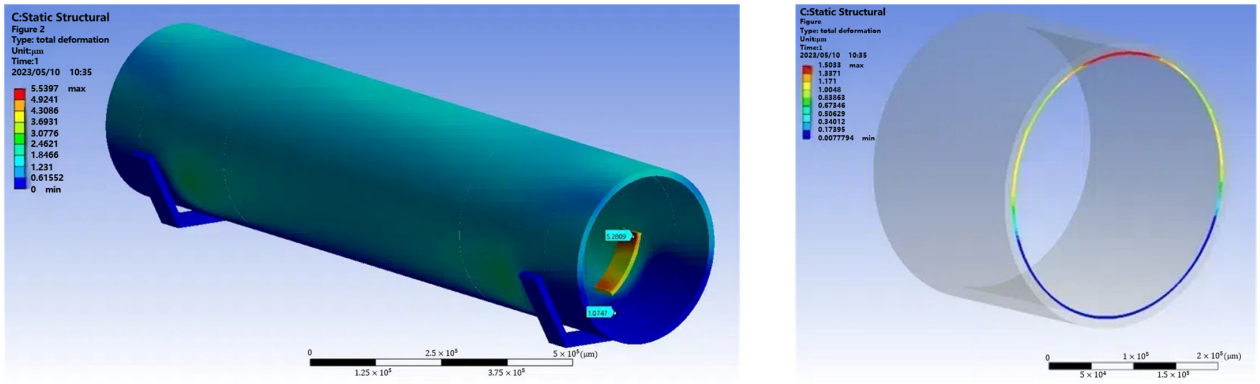

Figure 16. Cross-section deformation simulation.

Furthermore, during measurement, the pipe prover is empty, but in actual use, it is filled with liquid, creating a different measurement environment. Set the internal pressure of the volume tube according to the density of the medium when the pipe prover is actually used. The full-load hydraulic deformation of the pipe prover was simulated as shown in Figure 17, revealing a hydraulic deformation error of 0.2 µm.

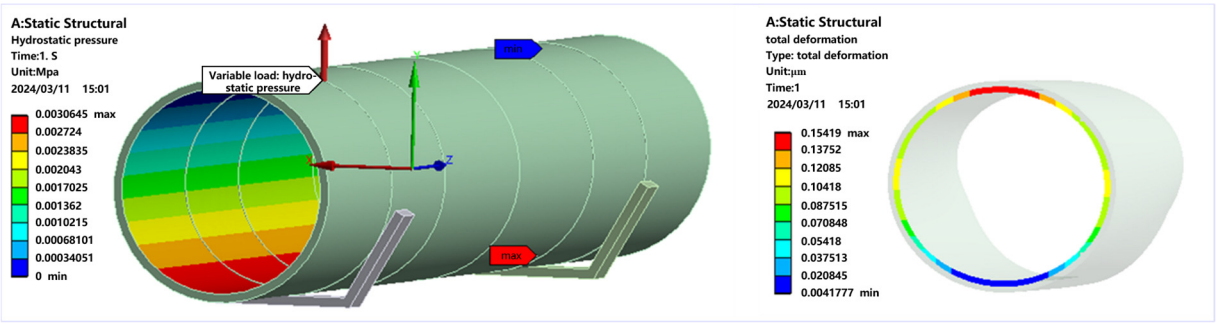

Figure 17. Cross-section hydraulic deformation simulation.

Throughout the measurement process, the environmental temperature fluctuated within a range of 2 °C. The sensor used for temperature compensation had an accuracy of ±0.1 °C. Considering that the wall thickness of the pipe prover was 40 mm, the thickness of the standard ring gauge was 137 mm, the linear expansion coefficient of the material had an uncertainty of 20%, and the errors were uniformly distributed, the uncertainty in the inner diameter measurement can be calculated, as listed in Table 9.

Table 9. Uncertainty in inner diameter measurement.

Source	Error (µm)	Coverage Factor	Uncertainty (µm)	Proportion
Repeatability of the inner diameter measurement results u_{D1}	4.05	$\sqrt{10}$	1.28	8.71%
Indication error of the inner diameter measurement u_{D2}	1.85	$\sqrt{3}$	1.07	6.08%
Temperature compensation error of the standard ring gauge u_{D3}	0.19	$\sqrt{3}$	0.11	0.06%
Standard ring gauge linear expansion coefficient error u_{D4}	0.76	$\sqrt{3}$	0.44	1.03%
Standard ring gauge traceability u_{D5}	4.00	2	2.00	21.26%
Inner diameter error of the measurement results caused by pipe roundness u_{D6}	5.87	$\sqrt{3}$	3.39	61.08%
Pipe prover radial temperature compensation error u_{D7}	0.14	$\sqrt{3}$	0.08	0.03%
Pipe prover radial linear expansion coefficient error u_{D8}	0.55	$\sqrt{3}$	0.32	0.54%
Pipe prover pressure deformation error u_{D9}	0.80	$\sqrt{3}$	0.46	1.12%
Pipe prover hydraulic pressure deformation error u_{D10}	0.21	$\sqrt{3}$	0.12	0.08%

All of the uncertainty sources in Table 9 are considered to be independent of each other; therefore, the synthetic uncertainty u_D of the inner diameter measurement can be calculated as

$$u_D = \sqrt{\sum_{i=1}^{10} {u_{Di}}^2} = 4.25 \text{ µm}. \quad (14)$$

5.2. Uncertainty Analysis of Length Measurement

The length measurement of the pipe prover was determined by the detection switch positions along the axial direction, as shown in Figure 8. Therefore, the measured length of each pipe prover segment was the difference between the positions of the two detection switches, which can also be obtained using Equation (12). The repeatability of the pipe prover length is characterized by the repeatability of the two detection switches. The measured positions of the detection switches for each segment of the pipe prover are shown in Figure 18.

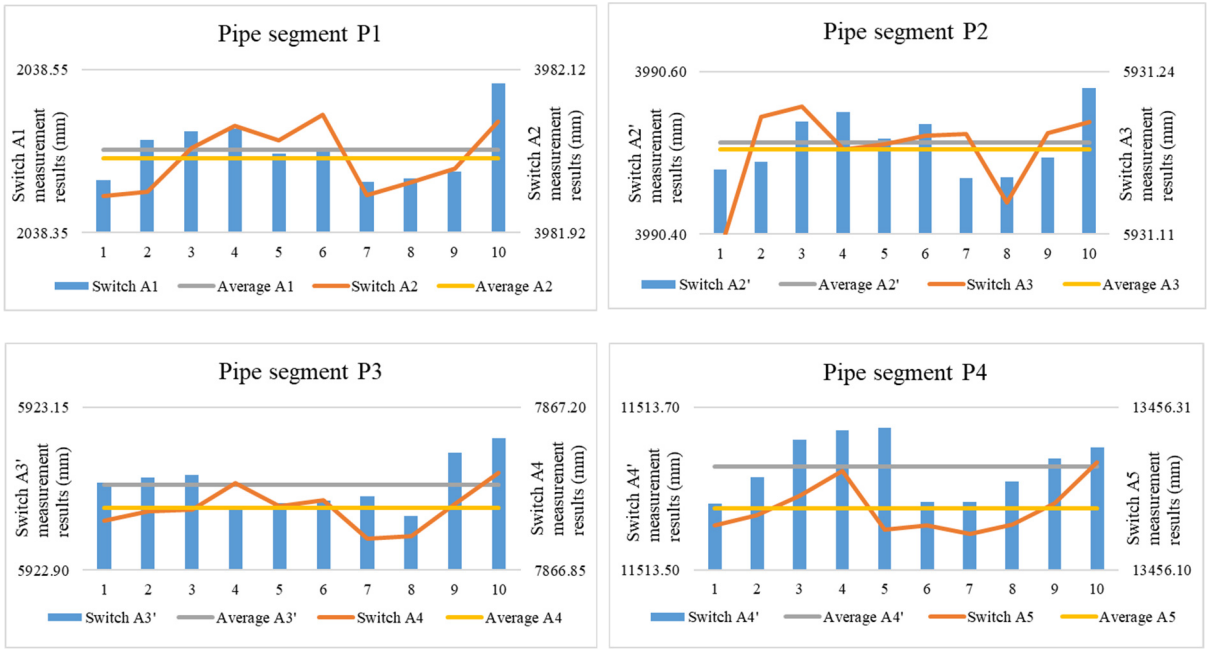

Figure 18. Position of pipe segment switches.

From this information, the repeatability of the detection switch of each pipe segment, repeatability of the volume pipe length measurement, and repeatability of the length measurement of each pipe segment can be obtained, as listed in Table 10.

Table 10. Length of pipe segment measurement uncertainty.

Pipe Segment	Switch Uncertainty (μm)	Length Uncertainty (μm)
P_1	11.94 12.54	17.32
P_2	11.96 11.14	16.34
P_3	12.08 14.04	18.52
P_4	11.74 10.34	15.65

The laser interferometer had an error indication. The expression of the indication error obtained after metrological verification is $(0.03 + 10^{-6}\ L)$ μm, where L is the measurement length in meters. The indication error is related to the measurement range L, so the indication error of each pipe segment is different.

When the device performs a length measurement, it must move to the detection switch position to trigger the switch and record the position at that moment. The measurement process is shown in Figure 19. However, due to a time delay (t = 1 ms) caused by the transmission of the trigger signal from the detection switch on the pipe prover to the

measurement device [28], and the measurement device moving at a speed v, an error occurs. When approaching the detection switch, the speed was set to v = 1 mm/s. This setting caused the laser interferometer to read the distance of the reflector located on the measurement device when the device was no longer at the triggering position of the detection switch. The error due to the time delay is equal to the product of this position difference and the speed.

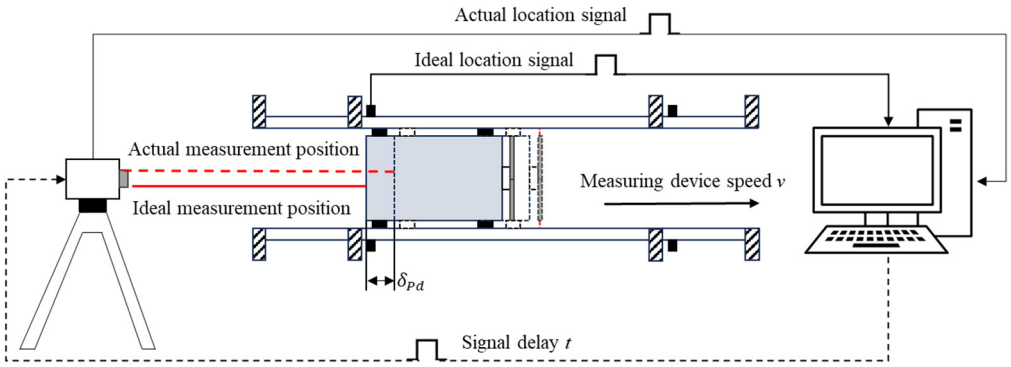

Figure 19. Principle of signal delay.

Throughout the measurement process, the ambient temperature fluctuated within 2 °C, and the sensor accuracy for temperature compensation was ±0.1 °C. Considering that the length of each segment of the pipe prover is as shown in Table 6 and the axial linear expansion coefficient of the pipe prover material is considered to have a 20% uncertainty, the uncertainty of the length measurement can be calculated as shown in Table 11.

Table 11. Uncertainty component in length measurement.

Source	P_1 (μm)		P_2 (μm)		P_3 (μm)		P_4 (μm)	
	Error	**Uncertainty**	**Error**	**Uncertainty**	**Error**	**Uncertainty**	**Error**	**Uncertainty**
Repeatability u_{L1}	17.32	17.32	16.34	16.34	18.52	18.52	15.64	15.64
Measurement error u_{L2}	2.59	1.50	3.59	2.07	4.70	2.71	5.81	3.36
Signal delay u_{L3}	1	0.58	1	0.58	1	0.58	1	0.58
Temp variation u_{L4}	3.36	1.94	3.36	1.94	3.36	1.94	3.36	1.94
Linear expansion coefficient u_{L5}	13.44	7.76	13.43	7.75	13.45	7.77	13.44	7.76

The length uncertainty of each pipe segment can be calculated separately by applying Equation (15):

$$u_{LP_j}(j = 1,2,3,4) = \sqrt{\sum_{i=1}^{5} u_{Li}{}^2}. \quad (15)$$

The length uncertainties for each pipe segment, u_{LP1}, u_{LP2}, u_{LP3}, and u_{LP4}, are listed in Table 12.

Table 12. Length measurement uncertainty.

Pipe Segment	Length Uncertainty (μm)
P_1	19.15
P_2	18.32
P_3	20.37
P_4	17.89

5.3. Pipe Prover Volume Uncertainty

From Equation (1) we can obtain the calculation formula for the pipe prover volume and then calculate the sensitivity coefficient formulas for the inner diameter and length, as shown in Equation (16):

$$\begin{cases} c_{LP_i} = \frac{\partial V_i}{\partial LP_i} = \frac{\pi}{4} \times DP_i (i = 1, 2, 3, 4) \\ c_{DP_i} = \frac{\partial V_i}{\partial DP_i} = \frac{\pi}{2} \times DP_i \times LP_i (i = 1, 2, 3, 4) \end{cases} \tag{16}$$

According to Tables 5 and 6, the sensitivity coefficients of each pipe segment can be calculated and are listed in Table 13.

Table 13. Sensitivity coefficient.

Pipe Segment	c_L (mm^2)	c_D (mm^2)
P_1	77,609.8934	959,690.8745
P_2	77,581.0594	958,083.6517
P_3	77,540.5822	959,456.1617
P_4	77,525.6281	958,672.7224

Then, combining Equation (1) with Table 1, the relative uncertainty of volume expansion (k = 2) can be found to be 0.012%.

6. Conclusions

In this study, we measured the volume of a pipe prover in situ using a dimensional method, which required determining the length and inner diameter of the pipe prover. We developed an algorithm model for the inner diameter measurement that was suitable for scenarios involving three measuring probes. This algorithm model was calibrated and verified using two standard ring gauges with different inner diameters, demonstrating its suitability for non-contact measurements. While parameters such as the angle, offset distance, and arm length of the inner diameter measurement module were challenging to measure directly, the experiment validated the accuracy of the method. The length measurements were completed using a laser interferometer, which enabled segmented measurements. The developed measurement device is compact and capable of comprehensive geometric measurements of the pipe prover. The difference between the measured and nominal pipe prover volumes was only 0.0066%. In future work, measuring the linear expansion coefficient of the volume tube could yield more accurate temperature compensation results. Additionally, we evaluated the measurement uncertainty of the device, finding that the relative expanded uncertainty of the volume measurement was only 0.012% (k = 2). Previously, the China National Institute of Metrology used the volumetric method to measure the pipe prover, and the measurement uncertainty reached 0.033%. Compared with this result, the measurement accuracy of the pipe prover measured by the dimensional method has been significantly improved. Thus, the proposed in situ measurement method effectively shortens the traceability chain and achieves a high level of accuracy in practical applications. An uncertainty analysis of the volumetric tube volume measured by the dimensional method was also performed, further affirming the method's reliability.

Author Contributions: Conceptualisation, J.H. and W.Z.; methodology, J.H. and A.C.; validation, W.Z. and J.C.; formal analysis, J.H., A.C., J.Y. and D.L.; investigation, W.Z., J.C. and Z.C.; resources, J.H., A.C. and D.L.; data curation, W.Z. and J.C.; writing—original draft preparation, W.Z.; writing—review and editing, W.Z. and J.H.; supervision, J.H. and A.C.; project administration, J.H. All authors have read and agreed to the published version of the manuscript.

Funding: Co-sponsored by the Key Laboratory of In-situ Metrology of the Ministry of Education (China Jiliang University) & Daqing Oilfield Design Institute (funding number: H221430).

Institutional Review Board Statement: Not applicable.

Informed Consent Statement: Not applicable.

Data Availability Statement: Data are available upon request.

Acknowledgments: The authors acknowledge the support provided by the Daqing Oilfield Design Institute for the experimental environment.

Conflicts of Interest: The authors declare no conflict of interest.

References

1. Hua, C.; Xie, C.; Xu, X. Follow-Up Control and Image Recognition of Neck Level for Standard Metal Gauge. *Appl. Sci.* **2020**, *10*, 6624. [CrossRef]
2. Doihara, R.; Shimada, T.; Cheong, K.H.; Terao, Y. Evaluation of Hydrocarbon Flow Standard Facility Equipped with Double-Wing Diverter Using Four Types of Working Liquids. *Metrologia* **2017**, *54*, 262. [CrossRef]
3. Castro, H.F.F. Mathematical modeling applied to the uncertainty analysis of a tank prover calibration: Understanding the influence of calibration conditions on the GUM validation using the Monte Carlo method. *Flow Meas. Instrum.* **2024**, *96*, 102547. [CrossRef]
4. Batista, E.; Paton, R. The Selection of Water Property Formulae for Volume and Flow Calibration. *Metrologia* **2007**, *44*, 453. [CrossRef]
5. Juliastuti, E.; Nadhira, V.; Zahra, N.; Muntafiah, D.; Suriasni, P.A. Laser Distance Meter for Cylinder Tank Volume Measurement System. In Proceedings of the Fourth International Seminar on Photonics, Optics, and Its Applications, Online, 1–2 December 2020; EDP Sciences: Les Ulis, France, 2021; Volume 11789, pp. 148–155.
6. Carmignato, S.; Savio, E. Traceable Volume Measurements Using Coordinate Measuring Systems. *CIRP Ann.* **2011**, *60*, 519–522. [CrossRef]
7. Doihara, R.; Shimada, T.; Cheong, K.H.; Terao, Y. Liquid Low-Flow Calibration Rig Using Syringe Pump and Weighing Tank System. *Flow Meas. Instrum.* **2016**, *50*, 90–101. [CrossRef]
8. Wright, J.D.; Nakao, S.I.; Johnson, A.N.; Moldover, M.R. Gas Flow Standards and Their Uncertainty. *Metrologia* **2022**, *60*, 015002. [CrossRef]
9. Mickan, B.; Strunck, V. A Primary Standard for the Volume Flow Rate of Natural Gas under High Pressure Based on Laser Doppler Velocimetry. *Metrologia* **2014**, *51*, 459. [CrossRef]
10. Shimada, T.; Doihara, R.; Terao, Y. Investigation into Calibration Performance of Small Volume Prover for Hydrocarbon Flow. *Flow Meas. Instrum.* **2015**, *41*, 174–180. [CrossRef]
11. Ogheard, F. Development of a Dynamic Gravimetric Calibration Method for Liquid Water Flow Metering. In Proceedings of the 19th International Congress of Metrology (CIM2019), Paris, France, 24–26 September 2019; EDP Sciences: Les Ulis, France, 2019; p. 17001.
12. Lim, K.W. A Study on the Measurement Uncertainty of Pipe Prover. *Trans. Korean Soc. Mech. Eng. B* **2000**, *24*, 1388–1398.
13. Oracheski, J.D.; Rausch, N. Tank volume measurement systems: Volume measurement uncertainty analysis. In Proceedings of the International Pipeline Conference, Calgary, AB, Canada, 4–8 October 2004; Volume 41766, pp. 2317–2343.
14. Morioka, T.; Ito, M.; Fujikawa, S.; Ishibashi, M.; Nakao, S.I. Development and evaluation of the calibration facility for high-pressure hydrogen gas flow meters. *Flow Meas. Instrum.* **2014**, *39*, 19–24. [CrossRef]
15. Chen, J.; Zhang, K.; Wang, L.; Yang, M. Design of a High Precision Ultrasonic Gas Flowmeter. *Sensors* **2020**, *20*, 4804. [CrossRef]
16. Prakosa, J.A.; Su, C.M.; Wang, W.B.; Sirenden, B.H.; Zaid, G.; Darmayanti, N.C.E. The Traceability Improvement and Comparison of Bell Prover as the Indonesian National Standard of Gas Volume Flow Rate. *MAPAN J. Metrol. Soc. India* **2021**, *36*, 81–87. [CrossRef]
17. Többen, H. Novel Technique for Calibration Pipe Prover Measuring. In Proceedings of the 11th IMEKO TC9 Conference on Flow Measurement, Groningen, The Netherlands, 12–14 May 2003.
18. Mahammad, S.A.; Chaudhary, K.P.; Yadav, S.; Sen, M.; Ghoshal, S.K. An Accurate Inner Diameter Measurement. *Rev. Sci. Instrum.* **2020**, *91*, 065112. [CrossRef]
19. Song, P.; Hu, L.; Chen, Y. Simulation Research on Three-Point Contact Outside Diameter Online Measuring Device. *J. Phys. Conf. Ser.* **2021**, *1952*, 032070. [CrossRef]
20. Dhanumalayan, E.; Joshi, G.M. Performance Properties and Applications of Polytetrafluoroethylene (PTFE)—A Review. *Adv. Compos. Hybrid Mater.* **2018**, *1*, 247–268. [CrossRef]
21. Kenny, D.A.; McCoach, D.B. Effect of the Number of Variables on Measures of Fit in Structural Equation Modeling. *Struct. Equ. Modeling* **2003**, *10*, 333–351. [CrossRef]
22. Tian, H.H.; Wang, Y.X.; Wang, H.X. Effect of Eccentricity on Roundness Measurement Accuracy for Cylindrical Components with Large Radius. *MAPAN J. Metrol. Soc. India* **2020**, *35*, 317–322. [CrossRef]
23. Shen, Y.; Ren, J.; Huang, N.; Zhang, Y.; Zhang, X.; Zhu, L. Surface Form Inspection with Contact Coordinate Measurement: A Review. *Int. J. Extreme Manuf.* **2023**, *5*, 022006. [CrossRef]
24. Arunthong, T.; Thuenhan, S.; Wongsripan, P.; Chomkokard, S.; Wongkokua, W.; Jinuntuya, N. Uncertainty Analysis of Linear Least Square Fitting Applied to Non-Linear Model. *J. Phys. Conf. Ser.* **2018**, *1144*, 012153. [CrossRef]

25. Alexander, D.L.; Tropsha, A.; Winkler, D.A. Beware of R^2: Simple, Unambiguous Assessment of the Prediction Accuracy of QSAR and QSPR Models. *J. Chem. Inf. Model.* **2015**, *55*, 1316–1322. [CrossRef]
26. Fan, K.C.; Wang, N.; Wang, Z.W.; Zhang, H. Development of a Roundness Measuring System for Microspheres. *Meas. Sci. Technol.* **2014**, *25*, 064009. [CrossRef]
27. Morii, H.; Masuta, H.; Kimura, H.; Sekimoto, M.; Kamiya, H. Development of Highly Accurate and Robust Roundness Measuring Instrument. *J. Phys. Conf. Ser.* **2018**, *1065*, 142007. [CrossRef]
28. Yuan, F. Performance Limits of Gated Delay Line Time Integrators. In Proceedings of the IEEE Canadian Conference on Electrical and Computer Engineering (CCECE), Halifax, NS, Canada, 18–20 September 2022; pp. 213–218.